CHIN. PHYS. LETT. Vol. 38, No. 12 (2021) 128501

High-Sensitivity Tunnel Magnetoresistance Sensors Based on Double Indirect and Direct Exchange Coupling Effect

Xiufeng Han(韩秀峰)[1,2*], Yu Zhang(张雨)[1,2], Yizhan Wang(王翼展)[1,2], Li Huang(黄黎)[1,2], Qinli Ma(马勤礼)[1,2], Houfang Liu(刘厚方)[1,2], Caihua Wan(万蔡华)[1,2], Jiafeng Feng(韦家峰)[1,2], Lin Yin(尹林)[1,2], Guoqiang Yu(于国强)[1,2], Tian Yu(余天)[3], and Yu Yan(闫羽)[4]

[1]*Beijing National Laboratory for Condensed Matter Physics, Institute of Physics, Chinese Academy of Sciences, Beijing 100190, China*
[2]*University of Chinese Academy of Sciences, Beijing 100049, China*
[3]*College of Physical Science and Technology, Sichuan University, Chengdu 610065, China*
[4]*Key Laboratory of Physics and Technology for Advanced Batteries (Ministry of Education), Department of Physics, Jilin University, Changchun 130012, China*

(Received 17 September 2021; accepted 3 November 2021; published online 18 November 2021)

Detection of ultralow magnetic field requires magnetic sensors with high sensitivity and low noise level, especially for low operating frequency applications. We investigated the transport properties of tunnel magnetoresistance (TMR) sensors based on the double indirect exchange coupling effect. The TMR ratio of about 150% was obtained in the magnetic tunnel junctions and linear response to an in-plane magnetic field was successfully achieved. A high sensitivity of 1.85%/Oe was achieved due to a designed soft pinned sensing layer of CoFeB/NiFe/Ru/IrMn. Furthermore, the voltage output sensitivity and the noise level of 10.7 mV/V/Oe, 10 nT/Hz$^{1/2}$ at 1 Hz and 3.3 nT/Hz$^{1/2}$ at 10 Hz were achieved in Full Wheatstone Bridge configuration. This kind of magnetic sensors can be used in the field of smart grid for current detection and sensing.

DOI: 10.1088/0256-307X/38/12/128501

Spintronic devices based on tunnel magnetoresistance (TMR) effect, which originates from the spin-dependent tunneling probability, have been widely explored in the last two decades since the giant TMR ratio with the magnitude of more than 200% is theoretically predicted[1,2] and experimentally demonstrated[3,4] in the MgO barrier magnetic tunnel junction (MTJ) at room temperature. The applications of MTJs with MgO barrier have been fully developed in magnetic random access memory (MRAM),[5–8] nonvolatile magnetic logic[9,10] and spin logic[8,11,12] and magnetic field sensors[13–18] due to the giant TMR ratio. For magnetoresistance (MR) sensors, their applications mainly focus on navigation,[19] nondestructive detection,[20] biomedical imaging,[21] and nanoparticle detection,[22] etc. However, the traditional MR sensor chips such as Hall sensors, anisotropic magnetoresistance (AMR) sensors and giant magnetoresistance (GMR) sensors cannot satisfy the requirements of the ultralow magnetic field detection. Meanwhile, with the advantages of high sensitivity and low noise level, the MgO based MTJ sensor[23] is highlighted as the most promising sensor aiming at pico-tesla magnetic field detection among the MR sensors at room temperature.

In practical applications, the deposited MTJ structure with collinear axis cannot be adopted for magnetic field sensors directly because of the sharp switching between parallel and anti-parallel magnetization configurations of two ferromagnetic layers, namely the free layer and reference layer, respectively. In order to realize the linear response to the external magnetic field, the magnetization of the free layer and reference layer of an MTJ are required to be orthogonal to each other. The shape anisotropy,[15,24] perpendicular magnetic anisotropy,[25,26] external field biasing,[27,28] superparamagnetic sensing layer[29,30] and double pinned MTJ structure[16,31,32] have been used to realize the desired orthogonal configurations. Nevertheless, the shape anisotropy needs large aspect ratio and the scheme of external field biasing increases the footprint in addition to power consumption. Perpendicular anisotropy is suitable for large dynamic range of measured magnetic field but owns a low sensitivity. While a superparamagnetic sensing layer usually needs an ultrathin ferromagnetic layer, leading to lower TMR ratio due to low spin polarization, which limits the sensitivity as well, the MTJ based on double indirect exchange coupling effect consists of a weakly pinned free layer via a nonmagnetic interlayer Ru and strongly pinned reference layer. With the proper annealing treatment procedure in magnetic field, the magnetization of free layer and reference layer will possess the orthogonal configuration. Thus, the ob-

Supported by the Framework Project of SGCC (Grant No. 5700-202058381A-0-0-00), and the National Key Research and Development Program of China (Grant No. 2017YFA0206200).
*Corresponding author. Email: xfhan@iphy.ac.cn
© 2021 Chinese Physical Society and IOP Publishing Ltd

tained MTJ provides the linear response to the external magnetic field without appealing to external field biasing or shape anisotropy. With the high sensitivity values, small footprint, low power consumption and ultralow-field detectivity, the double indirect exchange coupling structure is a more competitive scheme among others.

In this work, we studied the transport properties and intrinsic noise of MTJ sensors with the indirect exchange coupling structure for nano-tesla (nT) magnetic field detecting. The free layer and reference layer were pinned by IrMn and PtMn antiferromagnetic layers, respectively. The linear TMR effect was realized after two-step-annealing treatment in a high magnetic field. The MTJ sensors were connected in series-parallel[33] to reduce the low frequency noise, adjust the resistance value and improve robustness against external voltage/current impulses. As the MTJs were assembled into the Full Wheatstone Bridge configuration, the sensitivity of around 10.7 mV/V/Oe was achieved with the noise level of 10 nT/Hz$^{1/2}$ at 1 Hz and 3.3 nT/Hz$^{1/2}$ at 10 Hz. This work provided a competitive way for ultralow magnetic field detection and weak current sensing applications.

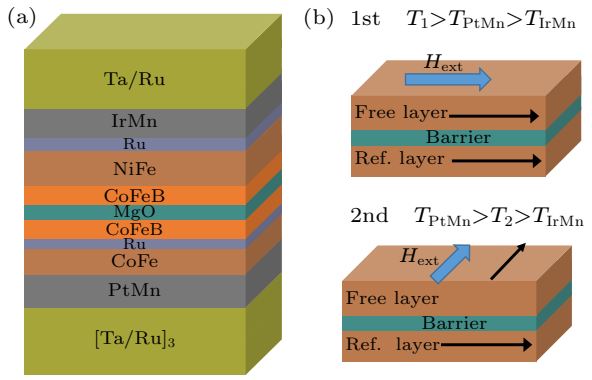

Fig. 1. (a) Schematic of the MTJ sensor stacks. (b) Schematics for the two-step annealing process. The 1st step is used to pin the reference layer by PtMn and the 2nd step is used to pin the free layer by IrMn. Proper annealing temperatures and field-directions are crucial to achieve the desired orthogonal relation between the reference and free layers.

Experiments. The MTJ films were deposited on thermally oxidized silicon wafers by an ultrahigh vacuum DC/RF magnetron sputtering system, with the structure of [Ta/Ru]$_3$/PtMn/CoFe/Ru/CoFeB/MgO/CoFeB/NiFe/Ru/IrMn/Ta/Ru [Fig. 1(a)]. The reference layer utilized the synthetic antiferromagnetic (SAF) structure to pin the magnetization of CoFeB and to reduce the magnetostatic interaction on the free layer. The composite free layer consisting of the CoFeB/NiFe/Ru/IrMn was aimed to lower saturation field, to obtain high TMR ratio simultaneously and thereby to achieve high sensitivity, where Ru acted as a structural blocking layer.[34] Then the films were patterned into micro-size junctions by the ultraviolet lithography and the subsequent argon ion etching. A two-step annealing process was adopted to obtain the desired orthogonal configuration as shown in Fig. 1. The antiferromagnetic PtMn and IrMn layers have higher and lower Neel temperatures, respectively. In the 1st annealing step, a higher temperature than the Neel temperature of PtMn was used and both reference and free layers were pinned along the external field. In the 2nd step, the sample was rotated by 90° respectively to the field and a temperature in between the Neel temperatures of PtMn and IrMn was used. In this case, the exchange bias direction of the reference layer pinned by PtMn will be maintained. Meanwhile, the free layer pinned by the IrMn layer was exchange-biased to another direction vertical to the previous one. Thus, the orthogonal relation between the reference and free layers was built [Fig. 1(b)]. After the two-step annealing process to obtain the linear output, the sensors were assembled on the Full Wheatstone Bridge configuration. The electrical transport was measured by the multi-source and meters (Keithley 2400 and Keithley 2182) and a 3D Helmholtz coil with the maximum field of 350 Oe and the resolution of 2 mOe at room temperature. The noise measurement was performed on low noise preamplifier (Stanford Research SR552) and low-pass filter (Stanford Research SR640), with the noise power spectrum density (S_V) calculated by the Fast Fourier Transform (FFT) averaged for 50 times.

Results and Discussion. The transmission electron microscope (TEM) characterization was performed to study the details of the MTJ structure. Figure 2(a) shows the cross-sectional HAADF (high-angle annular dark field) images, where the inset gives a simple structure schematic of the double pinned MTJ stacks. The clear interfaces indicate the good quality of the stack structure after two-step annealing. The Co and Fe elements shown in Figs. 2(b) and 2(c) are from the CoFe and CoFeB. In addition, the soft magnetic film NiFe also has the Fe element. The Ni element shown in Fig. 2(d) is only from the NiFe, which is used to soften the hybrid free layer and further to improve the sensitivity of sensor. Figure 2(e) shows the Mn element in the MTJ, which derived from the PtMn and IrMn layer. These two layers are used to pin the ferromagnetic layers. PtMn is employed for the SAF pinned reference layer and IrMn is for the composite free layer. The Mg element is from the MgO barrier and the O element from barrier and SiO_2 substrate. The B element has diffused into other layers from CoFeB after annealing process. The images of Mg, O and B in Figs. 2(f)–2(h) were not clear and confused with the other two elements, because they have small atomic numbers so that it was difficult to recognize them clearly in HADDF technique. These results confirm the MTJ sensor structures of our design.

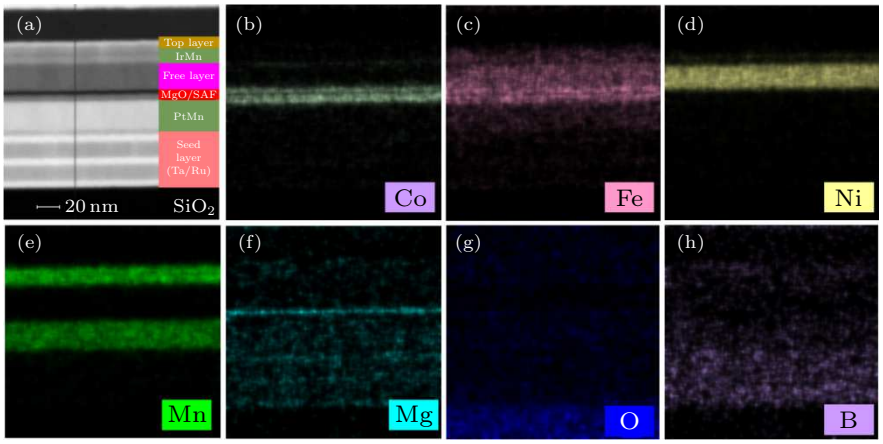

Fig. 2. Characterization of the MTJ structure. (a) The HAADF TEM image of the double pinned MTJ sensor, with the inset showing the details of the structure. (b)–(h) The corresponding EDS (energy dispersive spectrometer) mapping of the Co, Fe, Ni, Mn, Mg, O and B for the MTJ sensor.

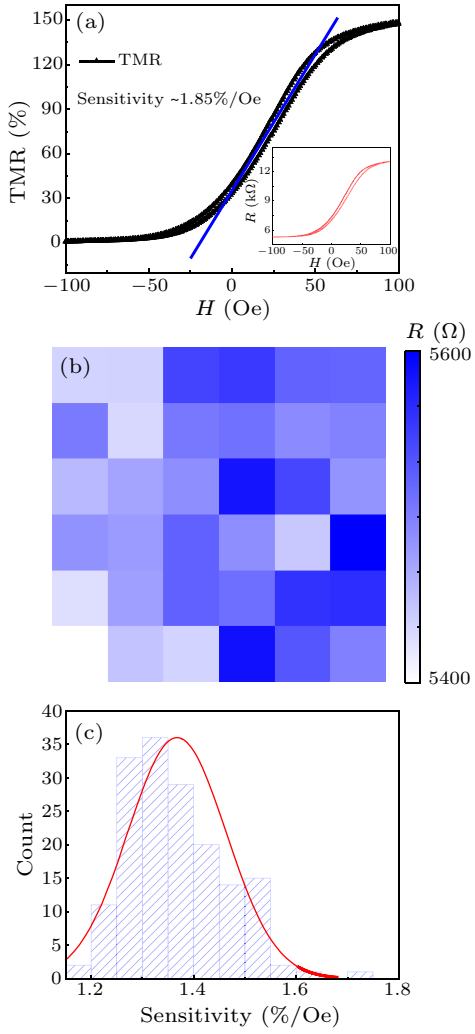

Fig. 3. (a) A typical field dependence of TMR ratio for a single-arm MTJ sensor. Its field dependence of resistance is shown in the inset. (b) and (c) Resistance and sensitivity distribution of 200 MTJs in the same wafer, indicating uniformity of the MTJs produced.

Figure 3(a) show the magnetic field dependence of the TMR ratio of a typical single-arm sensor which consists of several MTJ elements in series or in series-parallel connections. Here, TMR(H) is defined as $\mathrm{TMR} = [R(H) - R_\mathrm{P}]/R_\mathrm{P} \times 100\%$, where $R(H)$ and R_P are the resistance under certain magnetic field and the minimum resistance at the parallel state. The inset is the corresponding resistance R as a function of magnetic field. A TMR ratio of 150% was achieved, manifesting the high quality of our MTJ structures. If we defined the sensitivity as $\mathrm{TMR}/\Delta H$ in the linear range, the sensitivity would be as high as 1.85%/Oe, comparable with the highest results reported.[18] Figure 3(b) shows the R_P distribution of 200 MTJs in the same wafer, indicating uniformity of the sensors. Figure 3(c) summarized the sensitivity values for the 200 MTJs. An average value of 1.4%/Oe was achieved, also hinting the good uniformity performance of the MTJ sensors.

In industry applications, the Full Wheatstone Bridge has been widely used because it could realize the voltage output response directly and also alleviate the thermal drift effect.[35] Figure 4(a) shows the configuration of a Full Wheatstone Bridge which consists of four arms elements. Adjacent arms have the opposite dependence of resistance on external magnetic field. We used the input voltage as 1 V and the power consumption was only 10.75 μW according to $P = V^2/R$, where P is power, V is the input voltage and R is the resistance. The power consumption was much less than the AMR and GMR sensors.

The output of a Full Wheatstone Bridge structure is

$$\begin{aligned} V_\mathrm{out} &= V_+ - V_- \\ &= V_\mathrm{CC}\left(\frac{R_\mathrm{MTJ2}}{R_\mathrm{MTJ1}+R_\mathrm{MTJ2}} - \frac{R_\mathrm{MTJ4}}{R_\mathrm{MTJ3}+R_\mathrm{MTJ4}}\right), \end{aligned}$$

where V_out is the output voltage, V_+ and V_- are the voltage points after MTJ1 and MTJ3, as shown in Fig. 4(a), V_CC is the power supply voltage and R_i (i = MTJ1,..., MTJ4) is the resistance of the bridge

arm. Here, a voltage of 1 V was applied for testing. For practical applications, the input voltage could be from 1 V to 7 V. The voltage output sensitivity (S) of the Full Wheatstone Bridge is defined as $S = [V_{\rm out}/V_{\rm in}]/\Delta H$, where $V_{\rm in}$ is the input voltage and ΔH is the linear range. By structural tuning, S of 10.7 mV·V^{-1}·Oe^{-1} was obtained with ΔH of 50 Oe. S of the TMR sensors is comparable or higher than a typical AMR and GMR sensor with different field range ΔH.

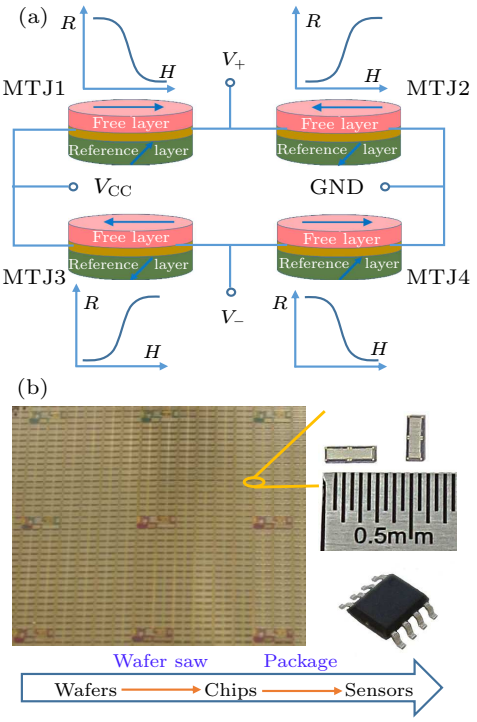

Fig. 4. (a) The schematic diagram of the TMR sensor which uses the Full Wheatstone Bridge configuration. (b) The left are partial optical images of MTJ sensor wafers, middle are half bridge chips with scale bar and the right are packaged sensors of high sensitivity MTJ sensors and each of them consists of two half bridge chips and an electro-static discharge chip.

For sensor application, the noise level is one of the critical parameters. The noise in MTJ sensor including thermal noise, shot noise, random telegraph noise (RTN) and $1/f$ noise.[36] For the thermal noise, there are two types: thermal electronic noise and thermal magnetic noise. The former results from the random motions of charge carriers because of temperature variations,[37,38] which is similar with Brownian motion. The thermal electronic noise is independent of frequency and its noise power spectrum density $S_{\rm thermal} = 4k_{\rm B}RT$, where $k_{\rm B}$ is the Boltzmann constant, R is the resistance and T is the testing temperature. The thermal magnetic noise is still under investigation and it is suggested that it results from the domain walls hopping between the free layer and reference layer with thermal excitation.[39] The $1/f$ noise also contains two types: electronic $1/f$ noise and magnetic $1/f$ noise. The electronic $1/f$ noise originates from the charge trapping of electronic in barriers and ferromagnetic layer,[40,41] while the magnetic $1/f$ noise is associated with thermally activated spin vibration of the free layer respective to the reference layer. It can also be attributed to the domain hopping between the metastable states.[42,43] Generally, the low-frequency noise ($1/f$ noise) is usually used to estimate the limitation of the detectivity of sensors.

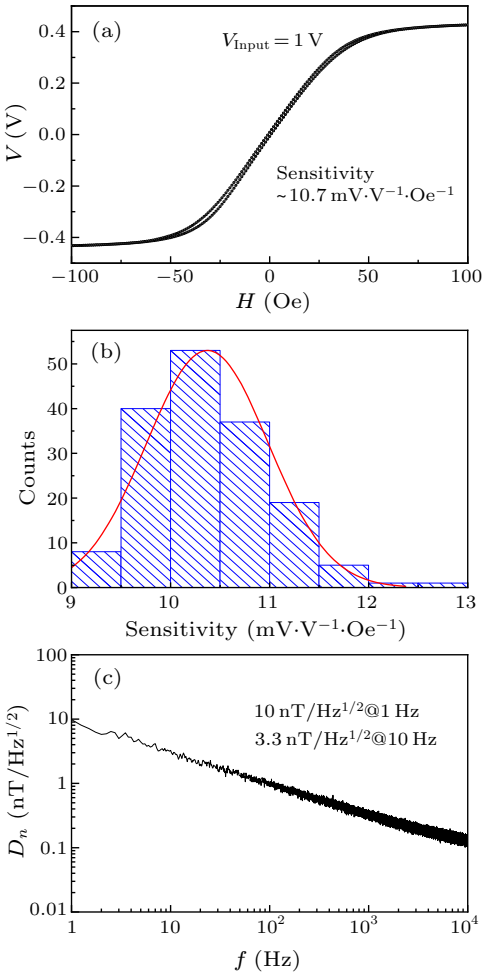

Fig. 5. (a) Field dependence of a magnetic sensor using the Full Wheatstone Bridge structure. (b) Sensitivity distributions of the sensors. (c) A typical noise spectrum of the sensor with 10 nT/Hz$^{1/2}$ at 1 Hz and 3.3 nT/Hz$^{1/2}$ at 10 Hz.

Figure 5 shows the field dependence of a TMR sensor and sensitivity distribution with the Full Wheatstone Bridge structure. Especially, a typical noise spectrum density as a function of frequency f is shown in Fig. 5(c). It is noted that the sensor noise is dominated by $1/f$ noise in the low frequency range. The minimum $S_{\rm V}$ of the noise testing system is on the order of 10^{-19} V^2/Hz, which was reported before.[18] The $S_{\rm V}$ of our sensor is on the order of 10^{-12}–10^{-13} V^2/Hz at 1 Hz, indicating the high accuracy. The detectivity (D_n) defined as $D_n = \sqrt{S_{\rm V}}/(S \cdot V_{\rm input})$ are 10 nT/Hz$^{1/2}$ at 1 Hz and 3.3 nT/Hz$^{1/2}$ at 10 Hz for our best sensor. The leakage current detection in smart grid, an important parameter to reflect the in-

sulation state of dielectric materials, is about μA→A level at 50 Hz or DC. The MTJ sensors would have a good prospect in leakage current nondestructive detection with the suitable magnetic field concentration technology.[44]

In summary, we have investigated the TMR sensors based on the double indirect exchange coupling effect. The MgO based MTJs with TMR ratio of about 150% was demonstrated in these specific structures with the sensitivities of 1.85%/Oe with the linear field range of 50 Oe. As assembled into Full Wheatstone Bridge, the best output sensitivity of 10.7 mV/V/Oe with the noise of 10 nT/Hz$^{1/2}$ at 1 Hz and 3.3 nT/Hz$^{1/2}$ at 10 Hz were achieved. Our results here demonstrate that the high sensitivity and low detecting field can be achieved in the double indirect exchange coupling structures, indicating that the design has been mature for the current detection in smart grid, artificial intelligence, automation control, automobile industry, household electrical appliances, and other industrial magneto-sensitive sensor applications.

References

[1] Butler W H, Zhang X G, Schulthess T C and MacLaren J M 2001 *Phys. Rev. B* **63** 054416
[2] Mathon J and Umerski A 2001 *Phys. Rev. B* **63** 220403(R)
[3] Parkin S S P, Kaiser C, Panchula A, Rice P M, Hughes B, Samant M and Yang S H 2004 *Nat. Mater.* **3** 862
[4] Yuasa S, Nagahama T, Fukushima A, Suzuki Y and Ando K 2004 *Nat. Mater.* **3** 868
[5] Diao Z, Apalkov D, Pakala M, Ding Y F, Panchula A and Huai Y M 2005 *Appl. Phys. Lett.* **87** 232502
[6] Gallagher W J and Parkin S S P 2006 *IBM J. Res. Dev* **50** 5
[7] Liu H, Wei H, Han X, Yu G, Zhan W, Le G S, Lu Y, Hehn M, Mangin S, Sun M, Liu Y and Horng C 2018 *Phys. Rev. Appl.* **10** 054013
[8] Kong W J, Wan C H, Guo C Y, Fang C, Tao B S, Wang X and Han X F 2020 *Appl. Phys. Lett.* **116** 162401
[9] Ikeda S, Hayakawa J, Lee Y M, Matsukura F, Ohno Y, Hanyu T and Ohno H 2007 *IEEE Trans. Electron. Devices* **54** 991
[10] Matsunaga S, Hayakawa J, Ikeda S, Miura K, Hasegawa H, Endoh T, Ohno H and Hanyu T 2008 *Appl. Phys. Exp.* **1** 091301
[11] Zhang X, Wan C H, Yuan Z H, Fang C, Kong W J, Wu H, Zhang Q T, Tao B S and Han X F 2017 *J. Magn. Magn. Mater.* **428** 401
[12] Kong W J, Wan C H, Wang X, Tao B S, Huang L, Fang C, Guo C Y, Guang Y, Irfan M and Han X F 2019 *Nat. Commun.* **10** 233
[13] Grancharov S G, Zeng H, Sun S H, Wang S X, O'Brien S, Murray C B, Kirtley J R and Held G A 2005 *J. Phys. Chem. B* **109** 13030
[14] Mao S N, Chen Y H, Liu F, Chen X F, Xu B, Lu P L, Patwari M, Xi H W, Chang C, Miller B, Menard D, Pant B, Loven J, Duxstad K, Li S P, Zhang Z Y, Johnston A, Lamberton R, Gubbins M, McLaughlin T, Gadbois J, Ding J, Cross B, Xue S and Ryan P 2006 *2006 IEEE Trans. Magn.* **42** 91
[15] Freitas P P, Ferreira R, Cardoso S and Cardoso F 2007 *J. Phys.: Condens. Matter* **19** 165221
[16] Yuan Z H, Huang L, Feng J F, Wen Z C, Li D L, Han X F, Nakano T, Yu T and Naganuma H 2015 *J. Appl. Phys.* **118** 053904
[17] Yuan Z H, Feng J F, Guo P, Wan C H, Wei H X, Ali S S, Han X F, Nakano T, Naganuma H and Ando Y 2016 *J. Magn. Magn. Mater.* **398** 215
[18] Huang L, Yuan Z H, Tao B S, Wan C H, Guo P, Zhang Q T, Yin L, Feng J F, Nakano T, Naganuma H, Liu H F, Yan Y and Han X F 2017 *J. Appl. Phys.* **122** 113903
[19] Caruso M J, Bratland T, Smith C H and Schneider R 1998 *Sensors* **15** 34
[20] Guo D W, Cardoso F A, Ferreira R, Paz E, Cardoso S and Freitas P P 2014 *J. Appl. Phys.* **115** 17E513
[21] Gaster R S, Xu L, Han S J, Wilson R J, Hall D A, Osterfeld S J, Yu H and Wang S X 2011 *Nat. Nanotechnol.* **6** 314
[22] Albon C, Weddemann A, Auge A, Rott K and Hutten A 2009 *Appl. Phys. Lett.* **95** 023101
[23] Ikeda S, Hayakawa J, Ashizawa Y, Lee Y M, Miura K, Hasegawa H, Tsunoda M, Matsukura F and Ohno H 2008 *Appl. Phys. Lett.* **93** 082508
[24] Lu Y, Altman R A, Marley A, Rishton S A, Trouilloud P L, Xiao G, Gallagher W J and Parkin S S P 1997 *Appl. Phys. Lett.* **70** 2610
[25] Mancoff F B, Dunn J H, Clemens B M and White R L 2000 *Appl. Phys. Lett.* **77** 1879
[26] Wei H X, Qin Q H, Wen Z C, Han X F and Zhang X G 2009 *Appl. Phys. Lett.* **94** 172902
[27] Liu X Y, Ren C and Xiao G 2002 *J. Appl. Phys.* **92** 4722
[28] Klaassen K B, Xing X Z and van Peppen J C L 2004 *IEEE Trans. Magn.* **40** 195
[29] Jang Y, Nam C, Kim J Y, Cho B K, Cho Y J and Kim T W 2006 *Appl. Phys. Lett.* **89** 163119
[30] Almeida J M and Freitas P P 2009 *J. Appl. Phys.* **105** 07E722
[31] Negulescu B, Lacour D, Montaigne F, Gerken A, Paul J, Spetter V, Marien J, Duret C and Hehn M 2009 *Appl. Phys. Lett.* **95** 112502
[32] Chen J Y, Feng J F and Coey J M D 2012 *Appl. Phys. Lett.* **100** 142407
[33] Guerrero R, Pannetier-Lecoeur M, Fermon C, Cardoso S, Ferreira R and Freitas P P 2009 *J. Appl. Phys.* **105** 113922
[34] Yuasa S and Djayaprawira D D 2007 *J. Phys. D* **40** R337
[35] Malinowski G, Hehna M, Montaigne F, Schuhl A, Duret C, Nantua R and Chaumontet G 2008 *Sens. Actuators A* **144** 263
[36] Lei Z Q, Li G J, Egelhoff W F, Lai P T and Pong P W T 2011 *IEEE Trans. Magn.* **47** 602
[37] Johnson J B 1928 *Phys. Rev. B* **32** 97
[38] Nyquist H 1928 *Phys. Rev. B* **32** 110
[39] Ingvarsson S, Xiao G, Parkin S S P, Gallagher W J, Grinstein G and Koch R H 2000 *Phys. Rev. Lett.* **85** 3289
[40] Weissman M B 1988 *Rev. Mod. Phys.* **60** 537
[41] Nowak E R, Weissman M B and Parkin S S P 1999 *Appl. Phys. Lett.* **74** 600
[42] Hardner H T, Huben M J and Tabat N 1999 *IEEE Trans. Magn.* **35** 2592
[43] Ren C, Liu X Y, Schrag B D and Xiao G 2004 *Phys. Rev. B* **69** 104405
[44] Gao K Z, Yin X L, Yang Y, Ewing D, De Rego P J and Liou S H 2020 *AIP Adv.* **10** 015301